

Computational Fluid Dynamics Simulation of a Nanofluid-Based Annular Solar Collector with Different Metallic Nano-Particles

Sireetorn Kuharat and O. Anwar Bég*

Aeronautical & Mechanical Engineering Department, School of Computing, Science and Engineering, Newton Building, University of Salford, Manchester, M54WT, UK.

Abstract

A numerical study of convective heat transfer in an annular pipe solar collector system is conducted. The inner tube contains pure water and the annular region contains nanofluid. Three-dimensional steady-state incompressible laminar flow comprising water-based nanofluid containing a variety of metallic nano-particles (copper oxide, aluminium oxide and titanium oxide nano-particles) is examined. The Tiwari-Das model is deployed for which thermal conductivity, specific heat capacity and viscosity of the nanofluid suspensions is evaluated as a function of solid nano-particle volume fraction. Radiative heat transfer is also incorporated using the ANSYS solar flux and Rosseland radiative models. The ANSYS FLUENT finite volume code (version 18.1) is employed to simulate the thermo-fluid characteristics. Mesh-independence tests are conducted. The influence of volume fraction on temperature, velocity, pressure contours is computed and visualized. Copper oxide nanofluid is observed to achieve the best temperature enhancement. Temperature contours at cross-sections of the annulus are also computed.

Keywords: *Thermal convection; nanofluid; annulus; ANSYS FLUENT; finite volume; metallic nano-particles; Temperature contours; Velocity; Pressure; Solar collector.*

Nomenclature

C_p	specific heat capacity	∇T	temperature gradient
k	thermal conductivity	μ_f	dynamic viscosity of base fluid
k_r	radiative conductivity	μ_{nf}	dynamic viscosity of nanofluid
n	refractive index	ρ	density
Q_c	thermal conduction flux	Φ	volume fraction
Q_{rad}	radiative flux term	$C_{p_{nf}}$	nanofluid specific heat
T	denotes temperature	ρ_f	base fluid density
V_f	volume of fluid	ρ_{nf}	nanofluid density
V_{np}	nano particles volume	ρ_s	nanoparticle density

1. Introduction

Motivated by cleaner and more sustainable energy resources in the 21st century, engineers have intensified efforts in studying and developing more efficient renewable energy designs. While many different options exist, solar energy remains the most promising owing to the vast quantities of heat received daily in many parts of the world. The current energy utilization globally is a fraction of the total solar radiation reaching the earth as noted by Kalogirou [1]. Solar collector design continues to undergo refinements and is being implemented on large scales in many continents. A wide spectrum of solar collectors has been implemented of which solar thermal absorption collectors (including concentrated solar power plants) are the most popular and absorb solar radiation directly via heating a working fluid which then drives a turbine connected to electrical generator units. These are the most widely deployed in commercial and domestic applications and include parabolic troughs, solar flat plate panels,

solar air heaters and solar towers and evacuated tube solar collectors, hybrid annular collectors etc. In all these systems, as opposed to photovoltaic systems, the “receiver” comprises conduits carrying the working fluid for thermal transfer. Depending on geographical locations different thermal collector designs are employed.

Laboratory and experimental testing of new solar devices is critical to their subsequent deployment. However, this can be a time-consuming and expensive endeavour. To improve predictions of projected efficiency, in parallel with field testing, theoretical and computational models currently provide the only feasible strategy and a relatively inexpensive method for optimization. Over the past four decades numerous different solar collector types have been studied with thermal fluid dynamic models. Lobo et al. [2] used numerical simulation is used to analyse the performance of an annular spaced cylindrical solar collector, comprising a transparent glass tube, mirrored over a segment of the circumference and engulfing the absorber tube for both an evacuated annular space and an air-filled one. Badran [3] reported both theoretical and experimental results for a novel tilted cylindrical-type solar collector comprising two steel cylinders with water filling the annular gap and the outside cylinder coated in plastic film glazing, with the ends of the cylinder being insulated. He considered strong solar flux cases with the annular gap heated and circulated via the thermo-syphonic driving force and achieved a maximum thermal efficiency of 85%. Bhutka et al. [4] used Meteororm software to investigate the performance of a solar parabolic absorption collector, computing heat gain and energy generation and benchmarking with the actual data of a 1 MW Solar Thermal Plant and a 50 MW Parabolic Trough Power Plant. Further studies include Tiedeman [5] (who considered integral and conventional solar water heating collectors), Boonchom et al. [6] (helix tube solar collectors), Reddy [7] (double rectangular solar integrated enclosures with transparent insulation materials (TIM) coated with phase-change material (PCM)), Bhargava [8] (wall losses in a tubular solar collector/water heater), Ortega et al. [9] (interzonal heat transfer in fin-modified solar collector walls) and Bég et al. [10] (finite difference simulation of radiative-convective viscous flow in porous media annular hybrid solar collectors) and Bég et al. [11] (thermo-solutal convection boundary layers on titled solar collector plates with Soret and Dufour multi-diffusive phenomena). These studies were all confined to Newtonian fluids. However, both thermal convection and efficiency can passively be enhanced by modifying flow geometry and boundary conditions e.g. inlet and wall conditions (as exemplified in refs. [2]-[10]) or alternatively by enhancing working fluid thermophysical properties.

In the 1990s, Choi [12] and co-workers in the USA developed a novel approach to increasing efficiency of fluids deployed in heat transfer operations. They introduced nanofluids. Nanofluids are a very successful family of engineered fluids, which contain well-dispersed nanoparticles suspended in a stable base fluid. The presence of metallic nanoparticles (e.g. gold, silver, copper, aluminium etc) significantly improves the thermo-physical properties of the host fluid and generally results in a considerable boost in thermal conductivity, density, and viscosity of nanofluid compared with the original base (host) fluid. This modification in fundamental thermal properties has profound implications in influencing the convective heat transfer process. An impressive range of applications of nanofluids have been explored in the last decade or so and these aspects in addition to fabrication and different types of nanofluids (carbon nanotubes, nano-shells, nano-particles, nano-wires etc) are lucidly reviewed in Das et al. [13]. Wang and Majumdar [14] have focused specifically on heat transfer characteristics. Recently nanofluids have been utilized in peristaltic nano-pumps in medical engineering [15], pharmaco-dynamic delivery systems [16], petroleum drilling operations [17] and smart coating systems for offshore applications [18]. Two popular mathematical models have been developed in recent years for simulating nanofluid transport phenomena. These are the two-component

laminar four-equation non-homogeneous equilibrium model of Buongiorno [19] and the volume fraction model of Tiwari and Das [20]. The former features thermophoretic forces and Brownian motion dynamics as the key contributors to thermal conductivity enhancement and includes mass, momentum, energy and species conservation. The latter focuses more on the type and properties of nano-particles and permits the computation of nanofluid properties for specific metallic (e.g. zinc or copper oxide) or non-metallic (e.g. diamond, silicate) nano-particles. In the Tiwari-Das model the volume fraction is engineered to be up to 10 % which enables mechanical behaviour like the base fluid and nanoparticle contribution is simulated through volume fraction instead of in a separate species conservation equation. Both models have received extensive attention in recent years. For example, the Buongiorno model has been deployed in coating flows [21], biofuel cells [22] and bio-nano-polymer manufacturing fluid dynamics [23]. The Tiwari-Das model has been utilized in peristaltic thermal nano-pumps [24], nano-polymer fabrication dynamics [25], electro-kinetic microfluidics [26] and chemical engineering mixing processes [27].

In recent years nanofluids have received extensive attention in solar energy collector studies. Many excellent reviews have been communicated on various systems by Elsheikh et al. [28] (e.g. solar collectors (SCs), solar thermoelectric devices, solar water heaters, solar-geothermal combined cooling heating and power system (CCHP), photovoltaic/thermal (PV/T) systems etc), Muhammad et al. [29] (on stationary solar collectors), Abdin et al. [30] (nanofluid doped solar collectors, fuel cells, photocatalysis and solar photovoltaics, Tegart [31] (who has considered both solar nanotechnology and other renewables) and Wang et al. [32] (spectrophotometry of dispersion stability of Chinese ink-based nanofluid solar collectors). Recent experimental studies of solar nano-doped collectors include Kiliç et al. [33] (on titanium dioxide/water nanofluid flat plate solar collectors) and Sharafeldin and Gróf [34] (Cerium oxide-water nanofluid flat-plate solar collectors at three different volume fractions of 0.0167%, 0.0333% and 0.0666%). Numerical studies of nanofluid-based solar collectors have utilized a wide range of computational methodologies. MeteGenc et al. [35] presented a time-dependent model to evaluate the thermal inertia of each component of Aluminium oxide-nanofluid flat plate solar i.e. glass, trapped air, absorber and working fluid and computing the mass flow rates at different flow Reynolds numbers and volumetric concentrations. Further studies include Yousefi et al. [36], Haghshenas et al. [37] (multiphase nanofluid tubular collectors), Colangelo et al. [38] (Aluminium oxide diathermic oil nanofluids), Meibodi et al. [39] and Mahian et al. [40] (SiO_2 /Ethylene Glycol-water nanofluid flat plate solar collectors, Bianco et al. [41] (turbulent Aluminium oxide water nanofluid pipe collectors), Al-Nimr et al. [42] (nano-doped copper oxide two-layer solar ponds) and Mahian et al. [43] (mini-channel titanium dioxide water collectors). The complex geometry of many solar collectors is often best addressed with computational fluid dynamics (CFD) software. Notable among such commercial finite volume codes is ANSYS FLUENT. This code has been used by the authors in numerous multi-physical fluid dynamics and heat transfer studies in recent years including Newtonian viscous natural convection in two-dimensional solar thermal absorbers with different radiative flux models [44], film cooling of turbulent heat transfer [45], mass transfer following de-icing of commercial aircraft wings [46], three-dimensional gas turbine blade film cooling [47] and rocket mini-channel cooling and turbulent convective heat transfer [48]. ANSYS FLUENT (version 18.1) allows incorporation of the Tiwari-Das model via a multi-phase physics capability. Computations are conducted with the pressure-based solver. Three-dimensional steady state flow is studied. We employ the SIMPLE algorithm available in the ANSYS FLUENT CFD code. The current study addresses convective heat transfer in an annular pipe solar collector system comprising an inner tube containing pure water and an annular region containing metal-water nanofluid. Three different metallic nano-particles (copper oxide, aluminium oxide and titanium oxide nano-particles) are examined. Via the Tiwari-Das model

the thermal conductivity, specific heat capacity and viscosity for each metal-water nanofluid suspension is calculated as a function of solid nano-particle volume fraction. Radiative heat transfer is also incorporated using the ANSYS solar flux and Rosseland radiative models. The ANSYS FLUENT finite volume code [49] is employed to simulate the thermo-fluid characteristics. Mesh-independence tests are conducted. Extensive visualizations of the influence of volume fraction on temperature, velocity, pressure contours are presented.

2. Computational thermo-fluid dynamic mathematical model

The solar collector geometry to be studied is illustrated in Figure 1 in an (x,y,z) coordinate system. It comprises two concentric cylinders, the inner composed of copper and the outer composed of glass. The copper tube has inner diameter 22mm, thickness 3 mm and is of 1m in length and contains flowing water. This inner copper tube is submerged in metallic nanofluid confined in the annular space between the copper tube and an external glass tube with internal diameter of 51 mm and wall thickness of 2.25 mm with the same length (1m). There is no heat transfer through the top wall (adiabatic end condition). No slip boundary conditions are assumed on all walls of the cavity are considered as impermeable. The physical properties of the fluid assumed constant. The physical model is shown in Figure 1.

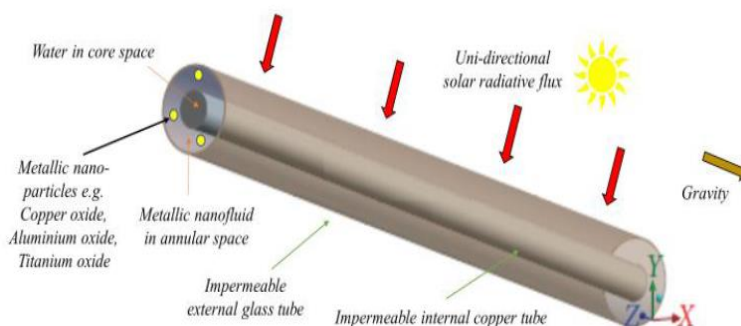


Figure 1. Geometrical and physical model for annular nanofluid solar collector.

The three-dimensional models of heat and fluid flow in the solar collector tube are designed in ANSYS FLUENT computational fluid dynamics software. Laminar, steady-state, incompressible flow is considered with forced convective heat transfer. The annular nanofluid is the absorber fluid and the Tiwari-Das nano-particle volume fraction model is deployed [20], which is described in due course. The fundamental equations for steady viscous, incompressible laminar flow are the three-dimensional time-independent Navier-Stokes equations, which in a Cartesian coordinate system, take the following form.

D'Alembert mass conservation (3-D continuity)

$$\left[\frac{\partial u}{\partial x} + \frac{\partial v}{\partial y} + \frac{\partial w}{\partial z} \right] = 0 \quad (1)$$

x-direction momentum conservation

$$\rho \left[u \frac{\partial u}{\partial x} + v \frac{\partial u}{\partial y} + w \frac{\partial u}{\partial z} \right] = \rho F_x - \frac{\partial p}{\partial x} + \mu \left[\frac{\partial^2 u}{\partial x^2} + \frac{\partial^2 u}{\partial y^2} + \frac{\partial^2 u}{\partial z^2} \right] \quad (2)$$

y-direction momentum conservation

$$\rho \left[u \frac{\partial v}{\partial x} + v \frac{\partial v}{\partial y} + w \frac{\partial v}{\partial z} \right] = \rho F_y - \frac{\partial p}{\partial y} + \mu \left[\frac{\partial^2 v}{\partial x^2} + \frac{\partial^2 v}{\partial y^2} + \frac{\partial^2 v}{\partial z^2} \right] \quad (3)$$

z-direction momentum conservation

$$\rho \left[u \frac{\partial w}{\partial x} + v \frac{\partial w}{\partial y} + w \frac{\partial w}{\partial z} \right] = \rho F_z - \frac{\partial p}{\partial z} + \mu \left[\frac{\partial^2 w}{\partial x^2} + \frac{\partial^2 w}{\partial y^2} + \frac{\partial^2 w}{\partial z^2} \right] \quad (4)$$

Forced convection takes place in the regime and the appropriate energy conservation equation is

$$u \frac{\partial T}{\partial x} + v \frac{\partial T}{\partial y} + w \frac{\partial T}{\partial z} = \alpha_m \left(\frac{\partial^2 T}{\partial x^2} + \frac{\partial^2 T}{\partial y^2} + \frac{\partial^2 T}{\partial z^2} \right) + Q_{rad} \quad (5)$$

Here, $\alpha_m = \frac{k}{\rho C_p}$ is the thermal diffusivity, which is a measure of thermal inertia. ANSYS FLUENT [50] provides a solar load model that can be used to calculate the radiation effects from the sun's rays that enters the computational domain. The Solar load is available in the 3D solver only and can be used to model both steady and unsteady flows. Two options are available for the model: Solar Ray Tracing and DO irradiation. Solar Ray Tracing is used in this simulation due to its highly efficient method and practical means of applying solar loads as heat sources in the energy equations. This study focuses on the *heat absorption capability* of various types of nanofluids, where the sun radiation is fixed in the z-direction along the pipe with the intensity of 877 W/m². The solar calculator utility in ANSYS FLUENT (solar load model) is turned off. Hence, the simulation can be easily recreated as a laboratory experiment. The solar load model's ray tracing algorithm can be used to predict the direct illumination energy source that results from incident solar radiation. This approach utilizes a beam that is modelled using the sun position vector and illumination parameters, applies it to any or all wall or inlet/outlet boundary zones specified, performs a face-by-face shading analysis to determine well-defined shadows on all boundary faces and interior walls and finally computes the heat flux on the boundary faces that result from the incident radiation. The solar ray tracing model includes only boundary zones that are adjacent to fluid zones in the ray tracing calculation. In other words, boundary zones that are attached to solid zones are ignored. The resulting heat flux that is computed by the solar ray tracing algorithm is coupled to the ANSYS FLUENT calculation via a source term in the energy equation (Q_{rad}). The heat sources are added directly to computational cells bordering each face and are assigned to adjacent cells in the following order: shell conduction cells, solid cells, and fluid cells. The solar ray tracing algorithm also accounts for internal scattered and diffusive loading. The reflected component of direct solar irradiation is tracked. A fraction of this radiative heat flux, called internally scattered energy is applied to all the surfaces participating in the solar load calculation, weighted by area. However, Solar Ray Tracing is not a *participating* radiation model. The model does not deal with emission from surfaces, and the reflecting component of the primary incident load is distributed uniformly across all surfaces rather than being local to the surfaces reflected. Since surface emission is also an important factor in this study, the Rosseland radiation model will be implemented in conjunction with Solar Ray Tracing. The Rosseland radiation model assumes that the intensity is the black-body intensity at the gas temperature. Since the radiative heat flux has the same form as the Fourier conduction law, it is possible to write

$$Q = Q_c + Q_r \quad (6)$$

$$= -(k + k_r) \nabla T \quad (7)$$

$$k_r = 16\sigma\Gamma n^2 T^3 \quad (8)$$

The appropriate substitution for radiative solar flux is made in the energy equation (5) to compute the temperature field. The Rosseland model has the advantage (compared with more complex alternative models (e.g. Chandrasekhar's discrete ordinates, the Trauggott P1 differential or Schuster-Schwartzchild two flux models as elucidated by Modest [51]) in that supplementary transport equation for the incident radiation do not have to be solved and this greatly accelerates computational speed and significantly less memory is required. However, the Rosseland model can be used only for optically thick media. It is recommended for use

when the optical thickness exceeds 3. In ANSYS FLUENT the Rosseland model is only available for the pressure-based solver, which is adopted in the present computations. Regarding the nanofluid modelling, the Tiwari-Das model [20] is employed which allows different concentrations (volume fraction) and types of metallic nano-particles. In ANSYS, this approach is implemented as a “one-phase flow” modification since the particles are very small. A nanofluid is defined in the ANSYS FLUENT workbench as a new fluid with a new density, viscosity, thermal conductivity and specific heat obtained as a function of a base fluid and nano-particle type and concentration (volume fraction), according to Brinkman [52], as used in [20]. The volume fraction can be estimated from

$$\phi = \frac{v_{np}}{v_f} \quad (9)$$

The dynamic viscosity can be estimated from

$$\mu_{nf} = \frac{\mu^f}{(1-\phi)^{2.5}} \quad (10)$$

The effective density and heat capacity also can be estimated from

$$\rho_{nf} = (1 - \phi)\rho_f + \phi\rho_s \quad (11)$$

$$C_{p,nf} = \frac{(1-\phi)(\rho C_p)_f + \phi(\rho C_p)_s}{\rho_{nf}} \quad (12)$$

The effective thermal conductivity of fluid can be determined by the Maxwell-Garnet relation which is adopted in Tiwari and Das [20].

$$\frac{k_{nf}}{k_f} = \frac{k_s + 2k_f - 2\phi(k_f - k_s)}{k_s + 2k_f - \phi(k_f - k_s)} \quad (13)$$

Here, k_{nf} = nanofluid thermal conductivity, k_f = fluid thermal conductivity and k_s = nanoparticle thermal conductivity. All calculated nanofluid properties (for the three different metallic nano-particles studied i.e. copper oxide, aluminium oxide and titanium oxide) are shown in the Appendix.

The transport equations (mass, momentum and energy) with nanofluid properties are solved subject to the boundary conditions in ANSYS FLUENT.

At the inlet: Volume flow rate inlet of 0.002 kg/s

At the outlet: Zero pressure outlet from one face.

Heat flux: Heat is added as the sun radiation intensity of 877 w/m² in solar load model.

The following volume fractions are considered each for the CuO, Al₂O₃ and TiO₂ nanofluids. 0.01wt%, 0.05wt%, 0.1 wt%. In ANSYS FLUENT physics, gravity is set as 9.81 m/s².

3. Ansys fluent grid sensitivity analysis

The annular solar collector mesh used a combination of unstructured grids (inner tube) and a structure grid (annulus) as shown in Figure 2. Hexahedral (“hex”) elements (finite volumes) are used in this simulation, as the hex mesh can provide the same resolution of the flow physics as tetrahedron mesh but with significantly fewer elements required. It is also important that the model does not contain any sliding mesh as this is not compatible with the solar load model.

Figure 3 illustrates the cross-section of the solar collector with mesh details. Figure 4 shows the grid sensitivity analysis. The largest elements used in case one can be considered as a coarse mesh with 103068 elements. On increasing the number of elements by 100000 (case two), the graph shows a variation indicating that the simulation is not convergent. Even though the difference between these two results is very small, nevertheless the heat convection is very sensitive to heat flux and cannot be ignored. The next part of the grid dependent study covers cases three, four and five. However, there is still some difference between the results of case

three and four. Further mesh refinement is therefore necessary and requires increasing the number of elements. Due to the limitation of student version of ANSYS software, the maximum number of elements available are 500,000. This forces the grid sensitivity study to stop at case five. Upon observation of cases four (325951 elements) and five (448836 elements), these cases utilize a fine mesh, where the difference between the two values are infinitesimal and hence considered negligible. This shows that the simulation is convergent at case four with 448836 elements. This grid-independence study provides an appropriate grid size (case four) which is subsequently adopted for all further simulations and is of sufficient quality to guarantee mesh-independent and converged results i.e. the most accurate results possible with the minimum number of elements.

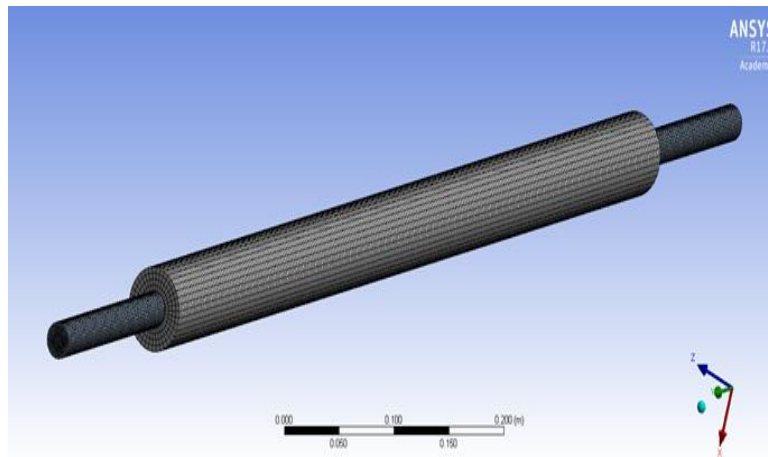


Figure 2. ANSYS FLUENT 3-dimensional mesh of solar configuration (Mesh density Nodes: 479188, elements: 443970).

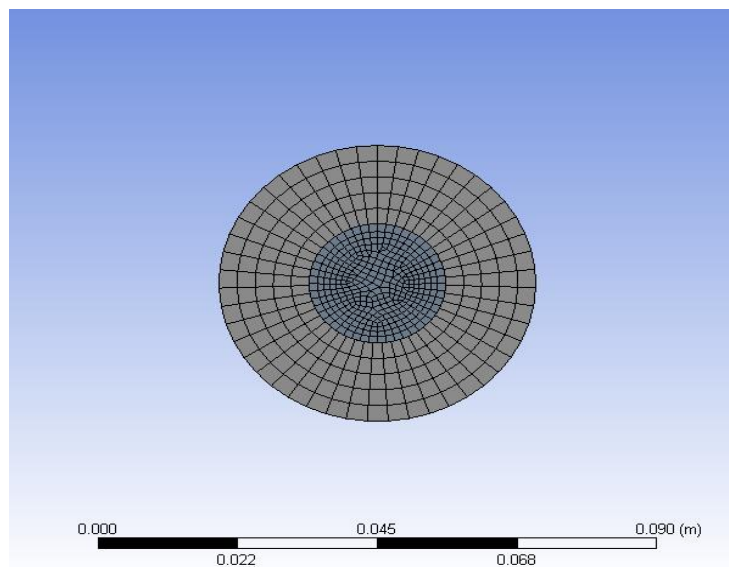


Figure 3. ANSYS FLUENT cross-sectional meshing details.

4. ANSYS FLUENT SIMULATION RESULTS

In the ANSYS simulations, T_w is the pipe wall temperature at a given location along the pipe and T_m is the mean temperature in the pipe at the location where T_w is defined. The ANSYS FLUENT results are depicted in Figures 5-13. Three different sets of results are visualized for the three metallic nano-particle cases i.e. Copper oxide, Aluminium oxide and Titanium oxide. In each of these three nanofluid cases, three different volume fractions are studied. Therefore

9 sets of computations are presented, three each for each different metallic nano-particle studied. We consider each set of three in turn. Volume fractions examined are $\phi = 0.01$, 0.05 and 0.1 i.e. 1%, 5% and 10%. Each set of figures illustrates respectively the temperature, temperature cross-section slice views, velocity and pressure distributions.

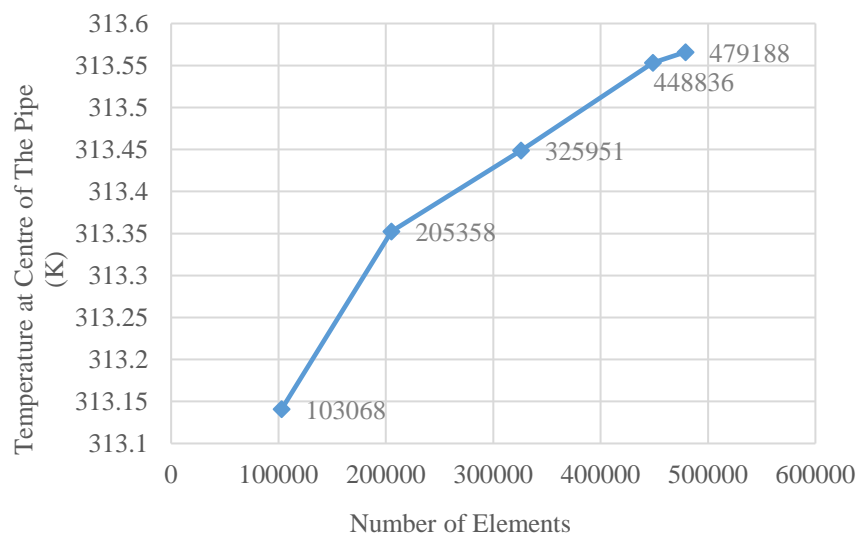


Figure 4. ANSYS FLUENT grid independence study.

Figures 5a-d to Figures 7a-d correspond to the Copper oxide case. Figures 5a-d correspond to $\phi = 0.01$, Figures 6a-d to $\phi = 0.05$ and Figures 7a-d to $\phi = 0.1$ respectively. To gain a perspective of the influence of volume fraction, one has to compare the respective plots with each other i.e. Figures 5a, 6a and 7a consider the temperature contours for copper oxide nanofluid with the three different volume fractions. Similarly, we compare Figures 5b, 6b and 7b (temperature cross-section slice views), then compare Figures 5c, 6c and 7c (velocity) and finally, Figures 5d, 6d and 7d (pressure distributions).

Figures 5a, 6a and 7a show a significant modification in temperature distributions as volume fraction is enhanced from $\phi = 0.01$, to $\phi = 0.05$ and finally $\phi = 0.1$. There is progressive heating from the base upwards of the annular region with increasing volume fraction. The blue zones are progressively eliminated, and green zones (higher temperature) extend further towards the upper adiabatic end. Red (maximum temperature zones) begin to appear at the highest volume fraction (Figure 7a). The increase in concentration of metallic nano-particles clearly enhances thermal conductivity of the nanofluid in the annular region and this intensifies thermal diffusion and heat transfer. Figures 5b, 6b and 7b (temperature cross-section slice views) provide a clearer visualization of the temperature at distinct locations in the annular space from the base of the solar collector to the top end (adiabatic end). There is a systematic evolution in contours. For the lowest volume fraction case, generally blue and green contours are prevalent (low temperatures) for the majority of the annular length. As volume fraction is increased, yellow and red zones are generated and become intensified towards the upper region of the annulus. Evidently therefore the enhancement in thermal conductivity encourages thermal diffusion and mobilizes a heating in the annulus indicating that more solar energy is captured, and that thermal efficiency is boosted (solar flux is fixed although it may be varied in the ANSYS specification). The presence of metallic nano-particles achieves an elevation in interfacial thermal conductivity and even in the absence of buoyancy forces (forced convection is considered) encourages significantly thermal absorption. These patterns are consistent with numerous other studies on metallic nanofluids including Moghadam et al. [53] and Maddah et al. [54]. Figures 5c, 6c and 7c illustrate the evolution in velocity through the annular space. A

less tangible influence is computed with increasing volume fraction. In all case high velocity zones arise at the inlet and outlet with slower zones in the interim sections. The primary influence on velocity is via the viscosity modification in the Tiwari-Das model. Although there is a slight intensification in velocity i.e. flow acceleration at the highest volume fraction (Figure 7c), this is only identified in the extremity zones of the annular geometry. Finally, pressure distributions are depicted in Figures 5d, 6d and 7d. Generally intermediate pressure is clearly computed (green zones) through the main body of the annulus at any volume fraction. There is a slight pressure drop at the extremities (corresponding to acceleration in the flow); however, the dominant influence of metallic nano-particles (copper oxide) is on the temperature field as noted earlier in Figures 5a, b, 6a, b and 7a, b. Effectively, the enhanced heat absorbed at high volume fraction in the annular nanofluid space is transferred via the inner copper cylinder to the central space (pure water) leading to an elevation in solar thermal efficiency.

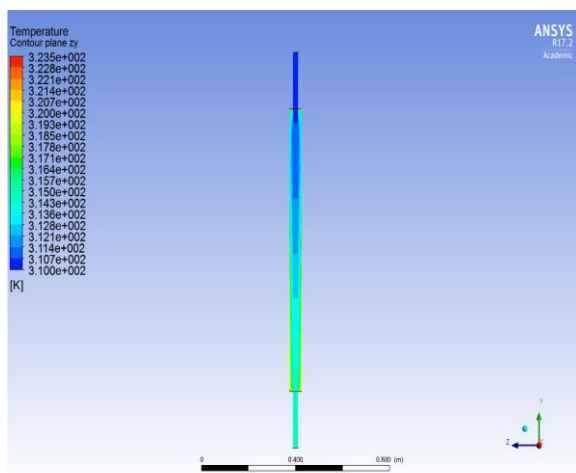


Figure 5a. Temperature Contour for CuO nanofluid, $\Phi = 0.01$.

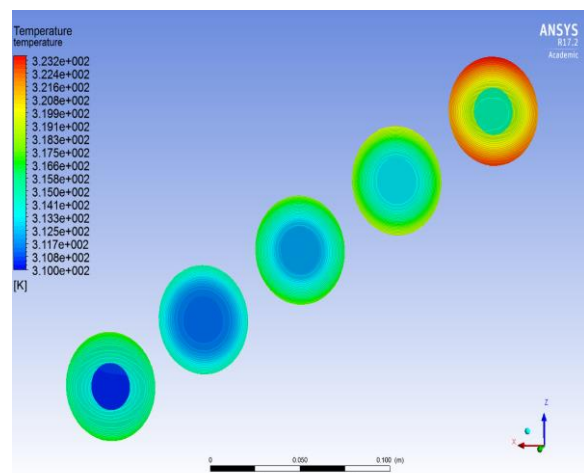


Figure 5b. Temperature Contour Cross-sections for CuO nanofluid, $\Phi = 0.01$.

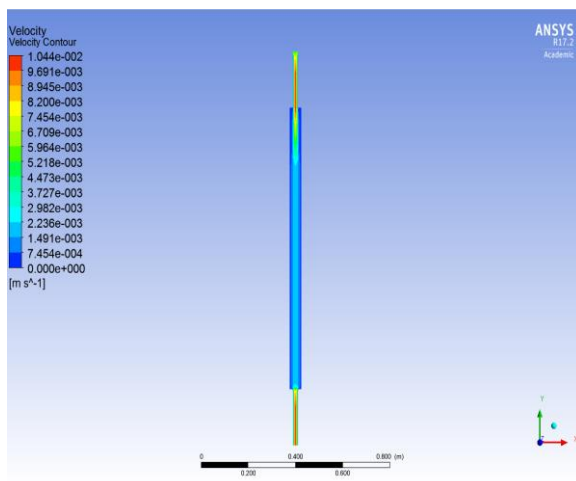


Figure 5c. Velocity Contours for CuO nanofluid, $\Phi = 0.01$.

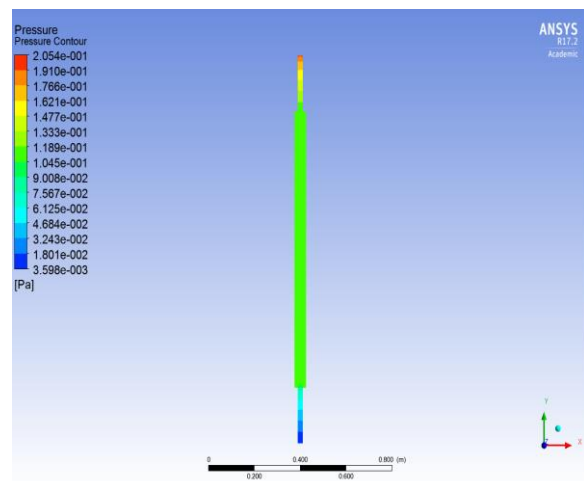


Figure 5d. Pressure Contours for CuO nanofluid, $\Phi = 0.01$.

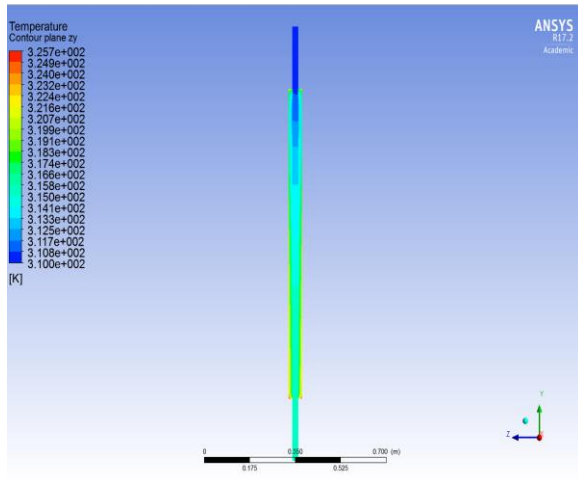


Figure 6a. Temperature Contour for CuO nanofluid, $\Phi = 0.05$.

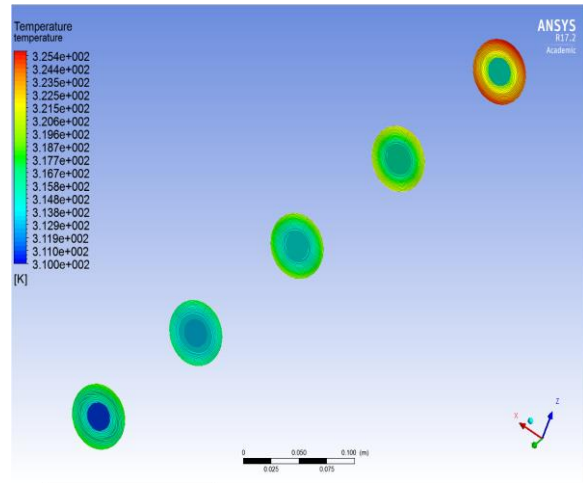


Figure 6b. Temperature Contour cross sections for CuO nanofluid, $\Phi = 0.05$.

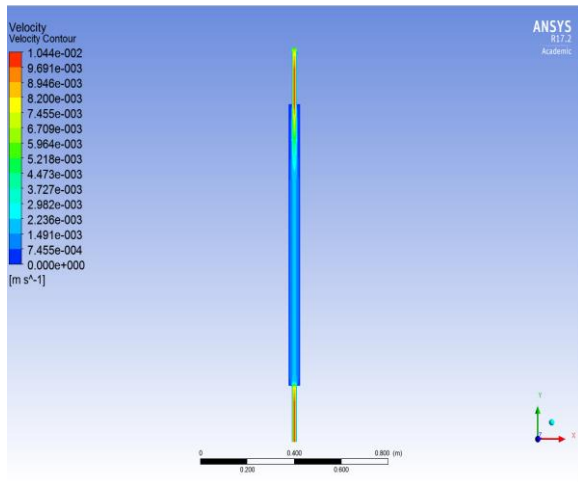


Figure 6c. Velocity Contours for CuO nanofluid, $\Phi = 0.05$.

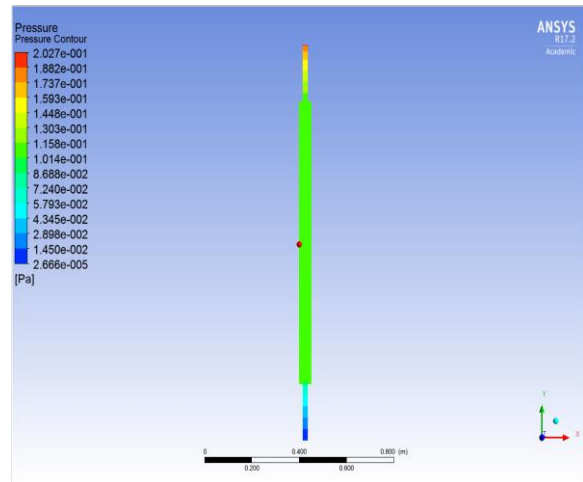


Figure 6d. Pressure Contours for CuO nanofluid, $\Phi = 0.05$.

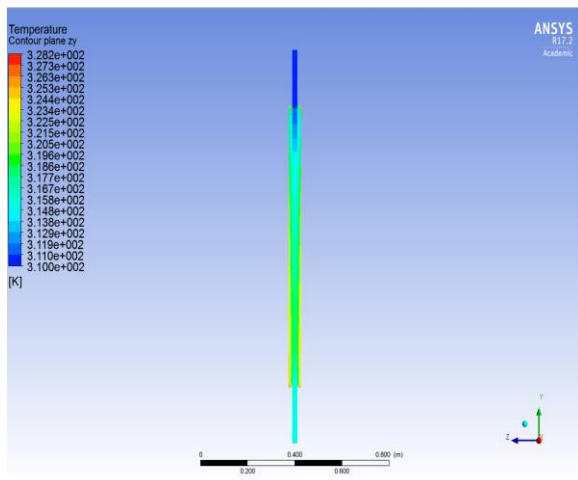


Figure 7a. Temperature Contour for CuO nanofluid, $\Phi = 0.1$.

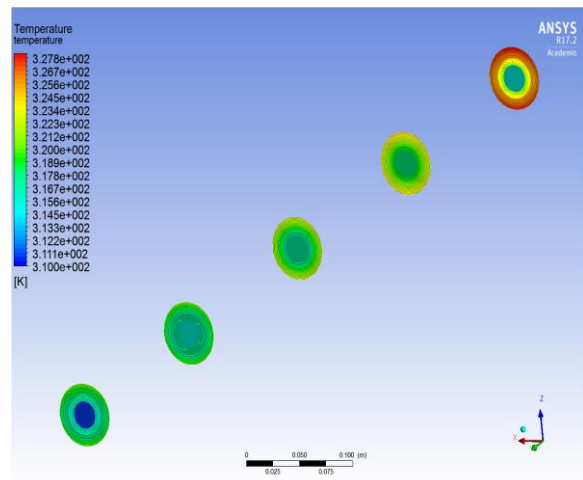


Figure 7b. Temperature Contour cross sections for CuO nanofluid, $\Phi = 0.1$.

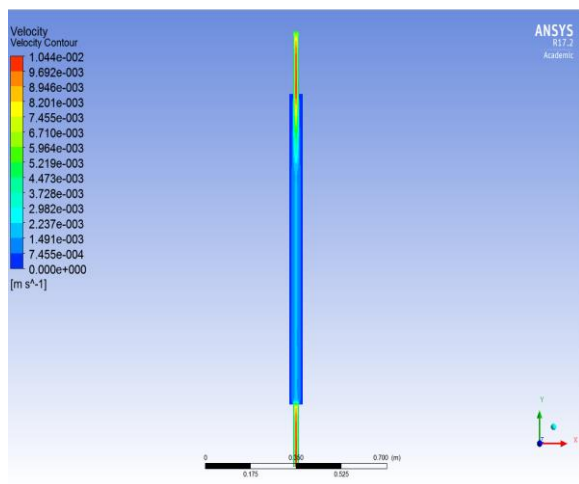


Figure 7c. Velocity Contours for CuO nanofluid, $\Phi = 0.1$.

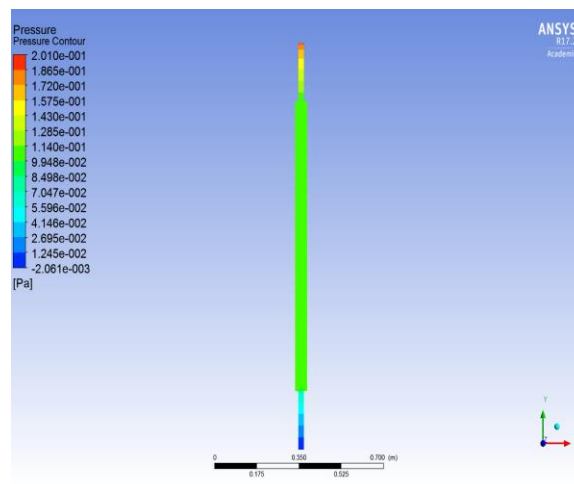


Figure 7d. Pressure Contours for CuO nanofluid, $\Phi = 0.1$.

Figures 8a-d to Figures 10a-c correspond to the Aluminium oxide nanofluid case, again at three different values of nano-particle volume fraction, viz $\phi = 0.01$, $\phi = 0.05$ and $\phi = 0.1$ respectively. Figures 8a, 9a, and 10a show a significant modification in temperature distributions as volume fraction is enhanced from $\phi = 0.01$, to $\phi = 0.05$ and finally $\phi = 0.1$. At lower volume fractions, there is a dominant blue zone throughout the main annular space with weak peripheral green zones (low temperatures). However, for the highest volume fraction, (Figure 10a) there is a marked growth in the green zone and emergence of yellow and very small red zones at the lower zone in the annulus, indicating that temperatures are increased, albeit weakly. Temperatures are, however, not as high as in the copper oxide cases (Figures. 5a, 6a and 7a) and this is probably attributable to the lower thermal conductivity of aluminium oxide compared with copper oxide. Inspection of the temperature cross-sections (Figures 8b, 9b and 10b) confirms the intensification in temperatures, in particular, near the periphery of the glass tube in the upper zone of the annulus with an increase in volume fraction. Progressively we observe the emergence of yellow zones in the later cross-sections at $\phi = 0.1$ which are absent at lower volume fractions. Darker blue and green zones vanish with stronger aluminium oxide nano-particle concentrations. However again there are lower temperatures achieved at the equivalent volume fraction for aluminium oxide compared with copper oxide (Figures 5b, 6b, 7b). Velocity is initially observed to be increased somewhat (Figures 8c, 9c) with increase in volume fraction from $\phi = 0.01$ to $\phi = 0.05$, especially in the inlet and outlet zones (blue slow zones are phased out with higher velocity green zones); however, with further elevation in volume fraction (Figure 10c) the trend is inhibited and there is a slight deceleration in flow near the upper zone of the annulus (inlet) and the re-emergence of blue zones. Negligible alteration in pressure is computed with an increase in volume fraction from $\phi = 0.01$ to $\phi = 0.05$ (Figures 8d and 9d) and further numerical experiments revealed that greater volume fractions of aluminium oxide nano-particles do not instigate any significant modification in pressure distributions.

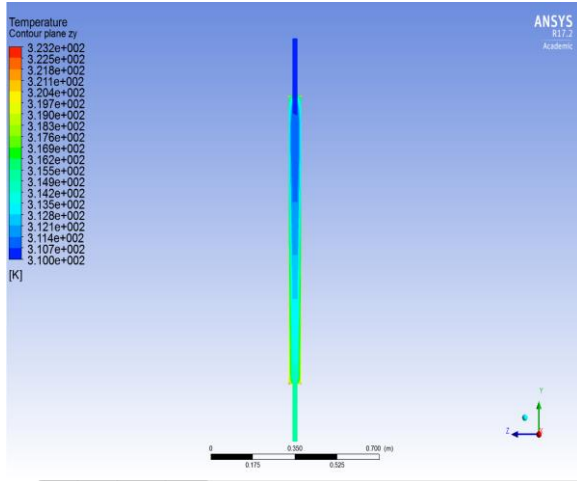


Figure 8a. Temperature Contour for Al_2O_3 nanofluid, $\Phi = 0.01$.

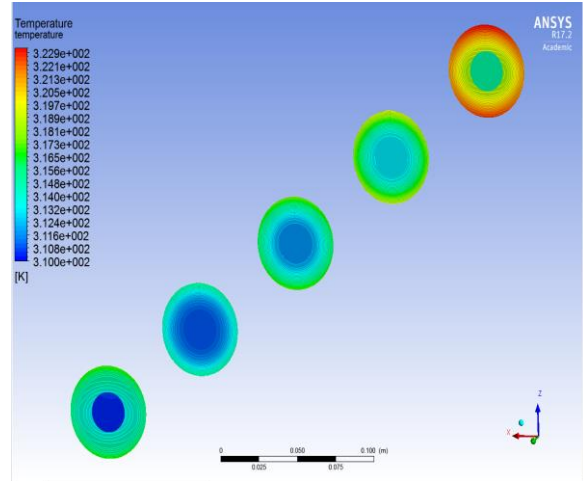


Figure 8b. Temperature Contour cross sections for Al_2O_3 nanofluid, $\Phi = 0.01$.

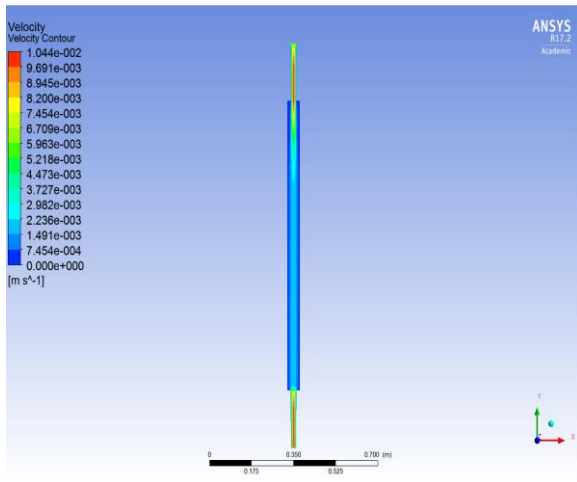


Figure 8c. Velocity Contours for Al_2O_3 nanofluid, $\Phi = 0.01$.

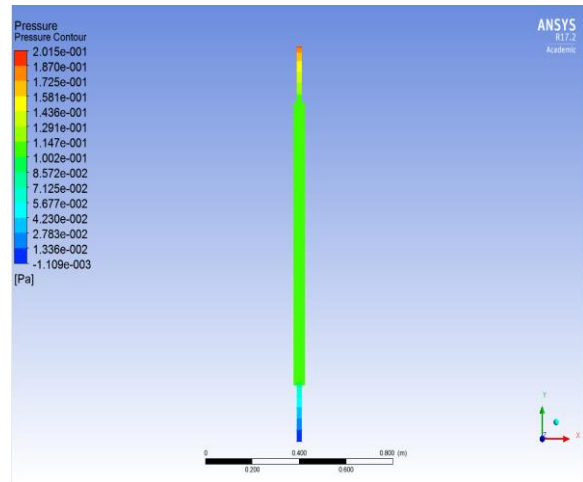


Figure 8d. Pressure Contours for Al_2O_3 nanofluid, $\Phi = 0.01$.

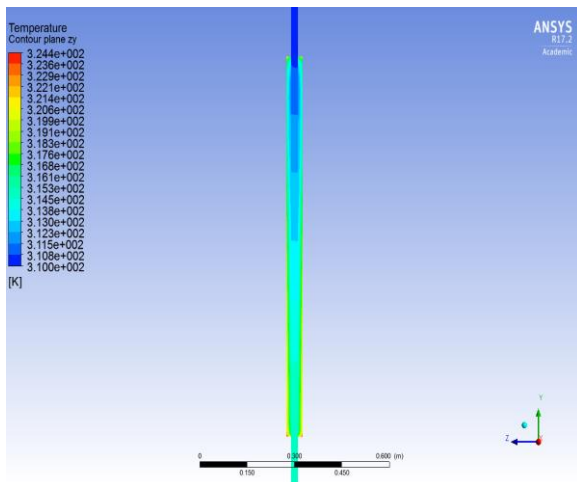


Figure 9a. Temperature Contours for Al_2O_3 nanofluid, $\Phi = 0.05$.

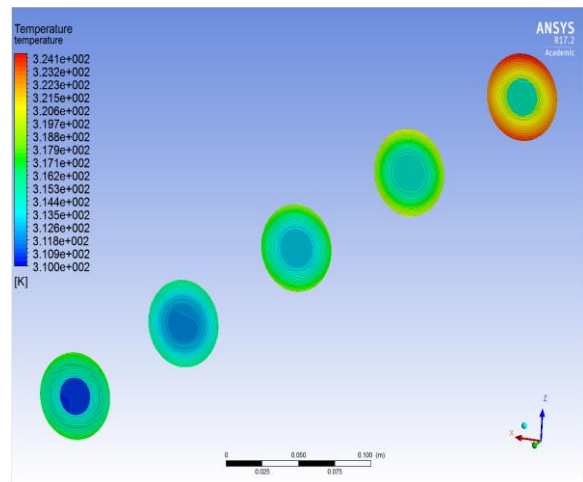


Figure 9b. Temperature Contour cross sections for Al_2O_3 nanofluid, $\Phi = 0.05$.

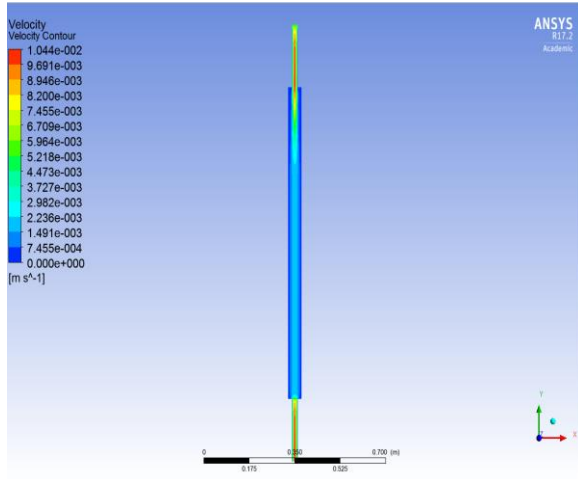


Figure 9c. Velocity Contours for Al_2O_3 nanofluid, $\Phi = 0.05$.

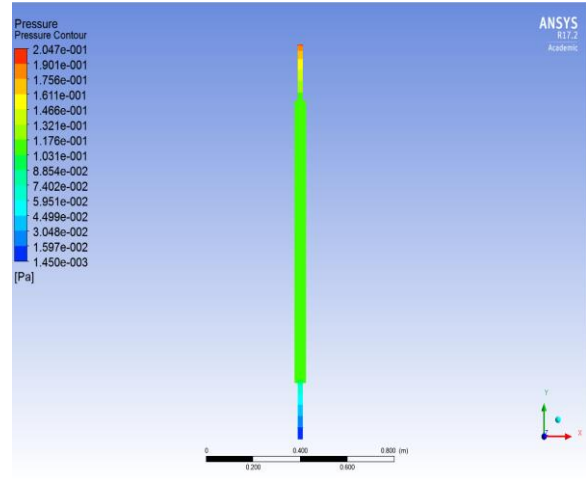


Figure 9d. Pressure Contours for Al_2O_3 nanofluid, $\Phi = 0.05$.

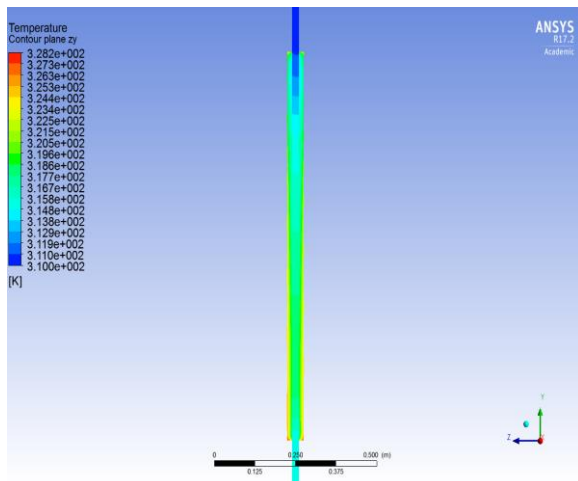


Figure 10a. Temperature Contours for Al_2O_3 nanofluid, $\Phi = 0.1$.

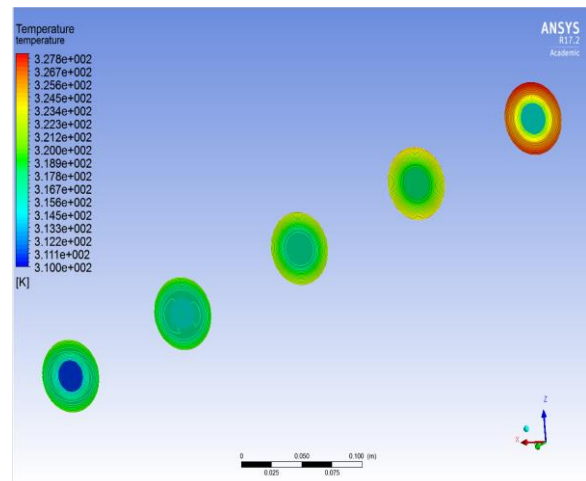


Figure 10b. Temperature Contour cross sections for Al_2O_3 nanofluid, $\Phi = 0.1$.

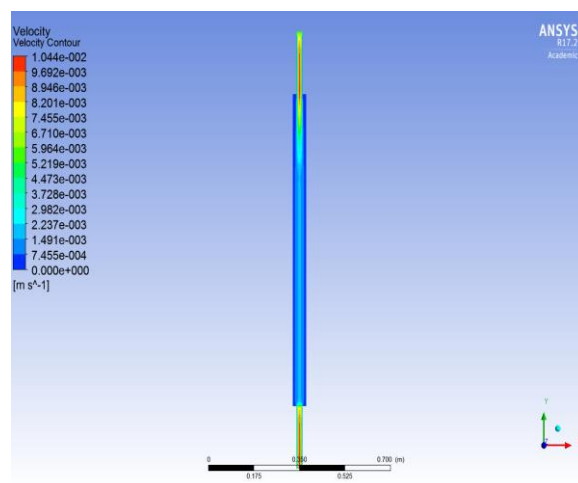


Figure 10c. Velocity Contours for Al_2O_3 nanofluid, $\Phi = 0.1$.

Figures 11a-d to Figures 13a-d correspond to the Titanium oxide nanofluid case, again at three different values of nano-particle volume fraction, viz $\phi = 0.01$, $\phi = 0.05$ and $\phi = 0.1$ respectively. Figures 11a, 12a and 13a show a significant increase in temperature magnitudes as volume fraction is enhanced from $\phi = 0.01$, to $\phi = 0.05$ and finally $\phi = 0.1$. At lower volume fractions, there is a prevalent blue zone (lowest temperatures) throughout the majority of the annulus with subsequent green zones (intermediate temperatures) as we approach the upper end and lower peripheral yellow zones (higher temperatures). However, as volume fraction is increased, (Figure 12a) there is a marked development in the green zone which extends further towards the upper end and a thickening in the yellow peripheral streaks with some presence of high temperature (red micro-zones at the base of the annulus). The temperatures are further increased for maximum volume fraction (Figure 13a) and the green zone extends yet further upwards with some yellow areas at the tube walls. The temperature magnitudes exceed those computed at the same values of volume fraction for Aluminium oxide (Figures 8a, 9a, 10a) but are substantially lower than those obtained for Copper oxide (Figures 6a, 6a, 7a). This confirms the superior performance of Copper oxide in achieving thermal enhancement in the solar annular collector. Figures 11b, 12b and 13b (temperature cross-section slice views) also show that temperatures are markedly enhanced with increasing volume fraction of titanium oxide nano-particles, as we progress from the lower end of the annular region to the upper end. Stronger red (high temperature) and yellow zones (quite high temperature) appear to grow considerably. The magnitudes achieved are larger than those for the Aluminium oxide cases (Figures 8b, 9b and 10b). However, they are still somewhat less than those attained for the Copper oxide cases (Figures 5b, 6b and 7b). Apparently therefore higher nano-particle concentrations (volume fractions) of Copper oxide attain the best thermal performance since the best absorption of solar thermal energy is achieved. Intensified thermal convection currents are generated for this case. Titanium oxide is the next best option, whereas Aluminium oxide is the least successful option. These findings are important since they generalize previous studies in which a single metallic nano-particle was examined e.g. Copper oxide by Moghadam et al. [53] or two metallic nanofluids (silver oxide and aluminium oxide) by Maddah et al. [54]. Figures. 11c, 12c and 13c visualize the velocity contours again for three different volume fractions. No substantial modification is generated in the velocities for the Titanium oxide case. Finally, pressure distributions are depicted in Figures 11d, 12d and 13d and it is evident that no tangible change arises in the pressure field with a change in volume fraction of titanium oxide nano-particles, concurring with the observations of Maddah et al. [54]. Finally, in Figure 14 we have presented residual iterations for the ANSYS FLUENT simulations for a sample case (Aluminium Oxide) indicating how excellent convergence is achieved and good accuracy is maintained.

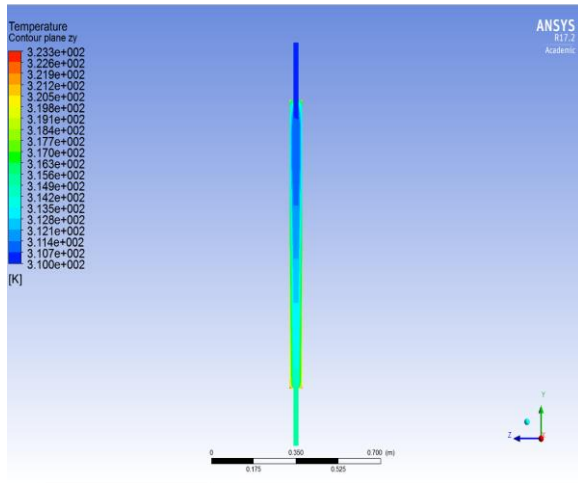


Figure 11a. Temperature Contours for TiO_2 nanofluid, $\Phi = 0.01$.

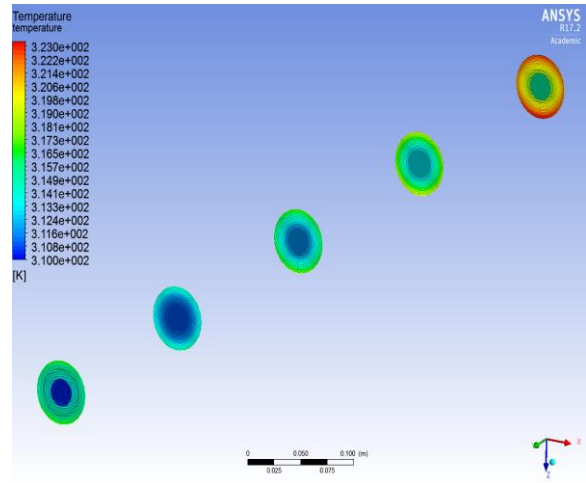


Figure 11b. Temperature Contour cross sections for TiO_2 nanofluid, $\Phi = 0.01$.

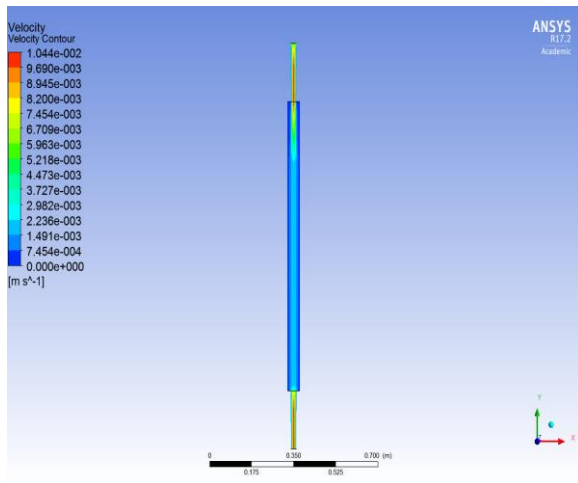


Figure 11c. Velocity Contours for TiO_2 nanofluid, $\Phi = 0.01$.

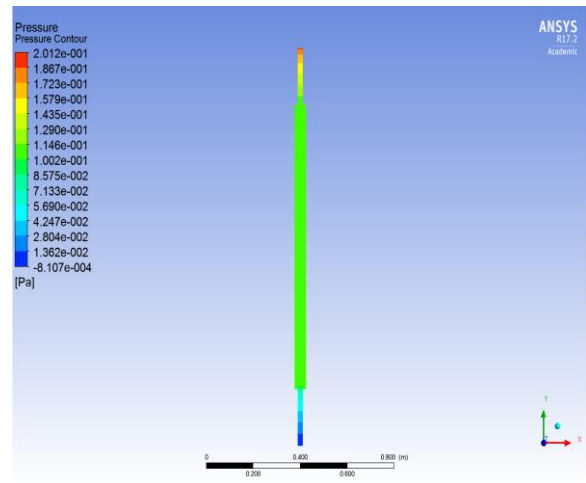


Figure 11d. Pressure Contours for TiO_2 nanofluid, $\Phi = 0.01$.

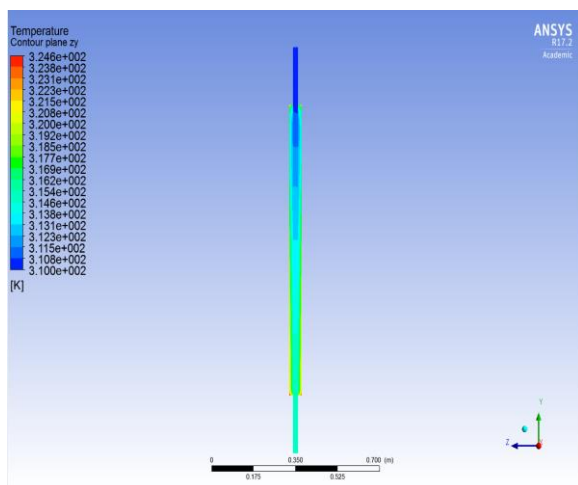


Figure 12a. Temperature Contours for TiO_2 nanofluid, $\Phi = 0.05$.

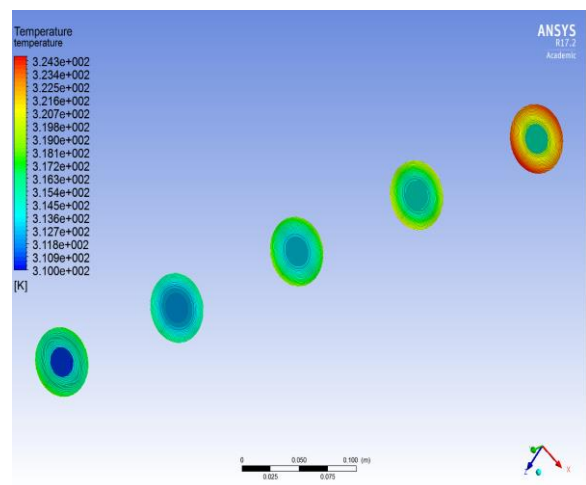


Figure 12b. Temperature Contours cross sections for TiO_2 nanofluid, $\Phi = 0.05$.

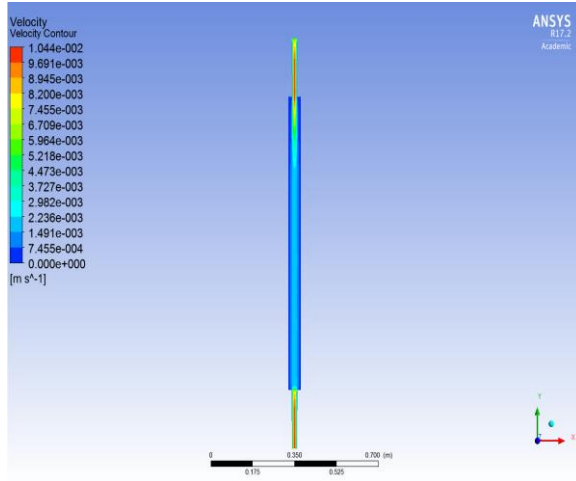


Figure 12c. Velocity Contours for TiO_2 nanofluid, $\Phi = 0.05$.

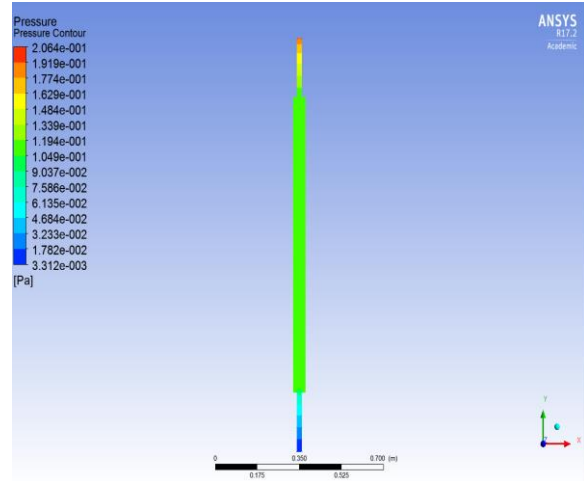


Figure 12d. Pressure Contours for TiO_2 nanofluid, $\Phi = 0.05$.

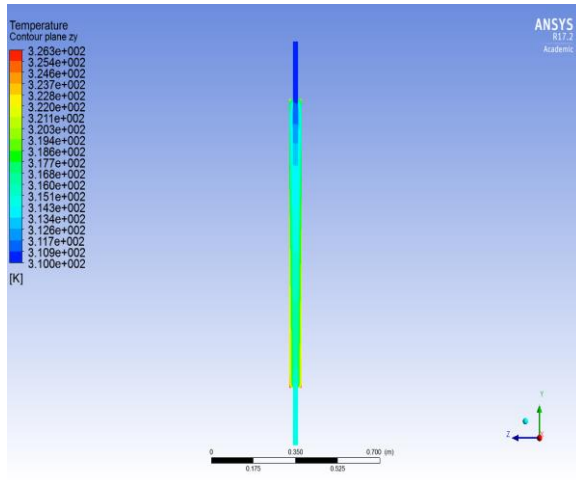


Figure 13a. Temperature Contours for TiO_2 nanofluid, $\Phi = 0.1$.

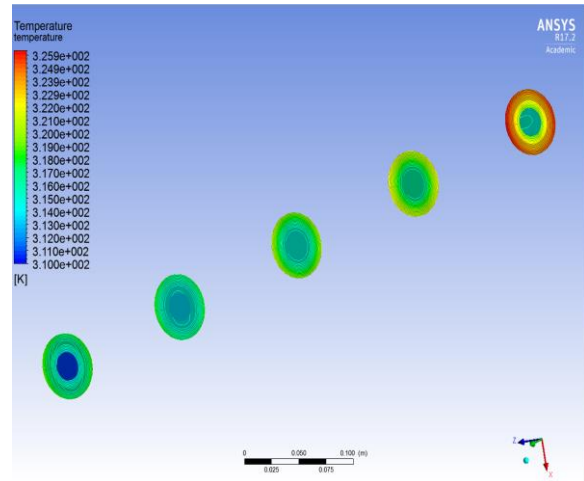


Figure 13b. Temperature Contour cross sections for TiO_2 nanofluid, $\Phi = 0.1$.

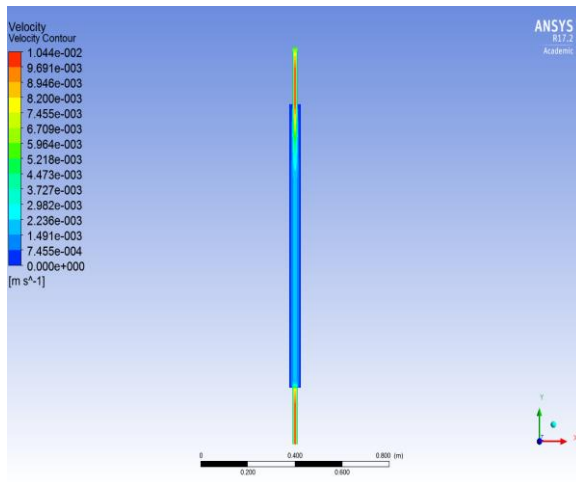


Figure 13c. Velocity Contours for TiO_2 nanofluid, $\Phi = 0.1$.

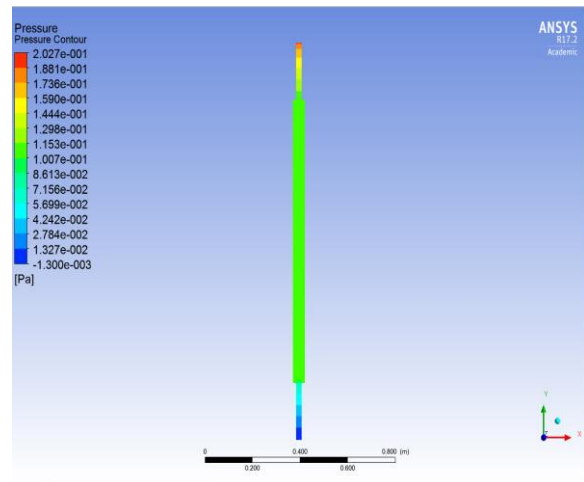


Figure 13d. Pressure Contours for TiO_2 nanofluid, $\Phi = 0.1$.

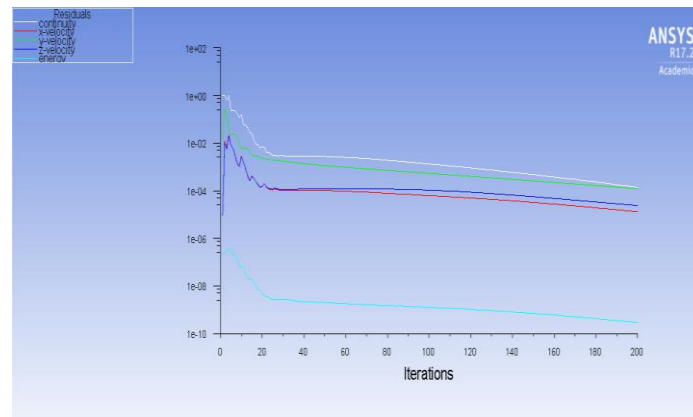


Figure 14. Residual iterations for ANSYS FLUENT simulation (TiO_2 nanofluid, $\Phi = 0.1$).

5. Conclusions

A computational simulation has been presented for forced convective heat transfer in an annular pipe solar collector system under solar radiative heat flux. ANSYS FLUENT 18.1 computational fluid dynamics software has been employed to analyse the three-dimensional steady-state incompressible laminar flow comprising water-based nanofluid containing a variety of metallic nano-particles (copper oxide, aluminium oxide and titanium oxide nano-particles). The Tiwari-Das model which utilizes the Maxwell-Garnett approach has been employed to simulate nanoscale effects. This model provides accurate expressions for thermal conductivity, specific heat capacity and viscosity of the nanofluid suspensions as a function of solid nano-particle volume fraction and is easily implemented in the FLUENT material physics option (under “one-phase flow”). Radiative heat transfer has been included via the ANSYS solar flux and Rosseland radiative models. Mesh-independence tests have been included. The influence of volume fraction on temperature, temperature cross-sections, velocity and pressure contours has been computed. The present analysis has shown that:

- (i) Copper oxide nanofluid is observed to achieve the best temperature enhancement. Temperature contours at cross-sections of the annulus are also computed.
- (ii) Titanium Oxide achieves higher temperatures than Aluminium Oxide but significantly lower temperatures than Copper Oxide.
- (iii) Temperature cross-sections exhibit significant enhancement in magnitudes with volume fraction for all three metallic nano-particles, although the best performance again is with Copper Oxide.
- (iv) There is flow acceleration for the Copper oxide case at the highest volume fraction although it is confined to the extremity zones of the annular geometry (inlet and outlet).
- (v) Velocities are initially increased with volume fraction for the Aluminium Oxide case but subsequently with maximum volume fraction they are reduced.
- (vi) Pressures are also reduced somewhat with increasing volume fraction for the Copper oxide case and not altered significantly for either Titanium Oxide or Aluminium Oxide cases.

The present study constitutes the first of a more general examination of annular nanofluid solar direct absorption collectors. Currently experiments are being designed in the Thermofluid Dynamics Laboratory at the University of Salford’s Mechanical and Aeronautical Engineering Department, to provide a compliment to the computational simulations and efforts in this regard will be communicated in the near future. Furthermore, alternative radiative heat transfer

models are being explored in ANSYS multi-physics and inclination of the annular solar collector is also an aspect of interest for future investigations.

Appendix -Nanofluid Properties

CuO		Al2O3		TiO2		Cu	
Vnp	1	Vnp	1	Vnp	1	Vnp	1
Vf	100	Vf	100	Vf	100	Vf	100
Φ	0.01	Φ	0.01	Φ	0.01	Φ	0.01
Pf	997.1	Pf	997.1	Pf	997.1	Pf	997.1
Ps	6500	Ps	3970	Ps	4250	Ps	8933
Pnf	1052.129	Pnf	1026.829	Pnf	1029.629	Pnf	1076.459
Cpf	4179	Cpf	4179	Cpf	4179	Cpf	4179
Cps	535.6	Cps	765	Cps	686.2	Cps	385
Cpnf	3953.913	Cpnf	4047.005	Cpnf	4034.828	Cpnf	3864.155
Ks	20	Ks	40	Ks	8.9538	Ks	401
Kf	0.613	Kf	0.613	Kf	0.613	Kf	0.613
Knf	0.618548	Knf	0.618801	Knf	0.617982	Knf	0.619042
uf	1.0798	uf	1.0798	uf	1.0798	uf	1.0798
unf	1.107275	unf	1.107275	unf	1.107275	unf	1.107275
CuO		Al2O3		TiO2		Cu	
Vnp	5	Vnp	5	Vnp	5	Vnp	5
Vf	100	Vf	100	Vf	100	Vf	100
Φ	0.05	Φ	0.05	Φ	0.05	Φ	0.05
Pf	997.1	Pf	997.1	Pf	997.1	Pf	997.1
Ps	6500	Ps	3970	Ps	4250	Ps	8933
Pnf	1272.245	Pnf	1145.745	Pnf	1159.745	Pnf	1393.895
Cpf	4179	Cpf	4179	Cpf	4179	Cpf	4179
Cps	535.6	Cps	765	Cps	686.2	Cps	385
Cpnf	3248.279	Cpnf	3587.525	Cpnf	3539.014	Cpnf	2963.277
Ks	20	Ks	40	Ks	8.9538	Ks	401
Kf	0.613	Kf	0.613	Kf	0.613	Kf	0.613
Knf	0.639772	Knf	0.640948	Knf	0.637125	Knf	0.642063
uf	1.0798	uf	1.0798	uf	1.0798	uf	1.0798
unf	1.227536	unf	1.227536	unf	1.227536	unf	1.227536
CuO		Al2O3		TiO2		Cu	
Vnp	10	Vnp	10	Vnp	10	Vnp	10
Vf	100	Vf	100	Vf	100	Vf	100
Φ	0.1	Φ	0.1	Φ	0.1	Φ	0.1
Pf	997.1	Pf	997.1	Pf	997.1	Pf	997.1
Ps	6500	Ps	3970	Ps	4250	Ps	8933
Pnf	1547.39	Pnf	1294.39	Pnf	1322.39	Pnf	1790.69
Cpf	4179	Cpf	4179	Cpf	4179	Cpf	4179
Cps	535.6	Cps	765	Cps	686.2	Cps	385
Cpnf	2648.545	Cpnf	3131.898	Cpnf	3056.457	Cpnf	2286.333
Ks	20	Ks	40	Ks	8.9538	Ks	401
Kf	0.613	Kf	0.613	Kf	0.613	Kf	0.613

Knf	0.664303	Knf	0.666458	Knf	0.659422	Knf	0.668496
uf	1.0798	uf	1.0798	uf	1.0798	uf	1.0798
unf	1.405196	unf	1.405196	unf	1.405196	unf	1.405196

References

- [1] S. A. Kalogirou, *Solar Energy Engineering*, 2nd Edition, Academic Press, USA, 2013.
- [2] P. C. Lobo, R. P. Kluppel and S. R. de Araujo, Performance of an annular cylindrical solar collector, *Proceedings of the International Conference*, Dhahran, Saudi Arabia, November 2-6, 1975.
- [3] A. A. Badran, Thermal performance of a cylindrical solar collector, *Energy Conversion and Management*, vol 32(3), pp. 217-222, 1991.
- [4] J. Bhutka, J. Gajjar and T. Harinarayana, Modelling of solar thermal power plant using parabolic trough collector. *Journal of Power and Energy Engineering*, vol 4, pp. 9-25, 2016.
- [5] F. T. Tiedeman, Side-by-Side Comparisons of Integral Collector Storage and Conventional Collector Solar Water Heating Systems, *ASME J. Sol. Energy Eng.*, vol 109(1), pp. 64-65, 1987.
- [6] K. Boonchom, A. Vorasingha, N. Ketiov and Threerachi Bongkarn, Performance evaluation of a helix tube solar collector system, *Int. J. Energy Res.*, vol 31, pp. 1169-1179, 2007.
- [7] K. S. Reddy, Thermal modelling of PCM-based solar integrated collector storage water heating system, *ASME J. Sol. Energy Eng.*, vol 129(4), pp. 458-464, 2007.
- [8] A. K. Bhargava, A simplified approach for evaluating performance of a solar water heater with side losses, *Int J Energy Research*, vol 7(1), pp. 81-92, 1983.
- [9] J. K. E. Ortega, C. E. Bingham and J. M. Connolly, Performance of storage walls with highly conductive covering plates and connecting fins, *ASME J. Sol. Energy Eng.*, vol 103(3), pp. 201-206, 1981.
- [10] O. Anwar Bég, N. Ali, A. Zaman, Eemaan T. A. Bég and Ayesha Sohail, Computational modelling of heat transfer in annular porous medium solar energy absorber with a P1-radiative differential approximation, *J. Taiwan Inst. Chemical Eng.*, vol 66, pp. 258-268, 2016.
- [11] O. Anwar Bég, A. Bakier, V. R. Prasad and S. K. Ghosh, Numerical modelling of non-similar mixed convection heat and species transfer along an inclined solar energy collector surface with cross diffusion effects, *World Journal of Mechanics*, vol 1, pp. 185-196, 2011.
- [12] S. Choi, Enhancing thermal conductivity of fluids with nanoparticles, *Proceedings of the ASME International Mechanical Engineering Congress and Exposition*, San Francisco, CA, 1995.
- [13] S. K. Das, S. U. S. Choi, W. Yu, and T. Pradet, *Nanofluids: Science and Technology*, Wiley, Hoboken, NJ, 2007.
- [14] X. Q. Wang, and A. S. Mujumdar, Heat Transfer Characteristics of Nanofluids: A Review, *Int. J. Therm. Sci.*, vol 46, pp. 1-19, 2007.
- [15] O. Anwar Bég, D. Tripathi, Mathematica simulation of peristaltic pumping with double-diffusive convection in nanofluids: A bio-nano-engineering model, *IMEchE Part N-J. Nanoengineering and Nanosystems*, vol 225, pp. 99-114, 2011.
- [16] D. F. Emerich, C. G. Thanos, The pinpoint promise of nanoparticle-based drug delivery and Molecular diagnosis, *Biomol Eng.*, vol 23, pp.171-184, 2006.
- [17] O. Anwar Bég, D. E. Sanchez Espinoza, Ayesha Sohail, A.Tasveer Bég and Ali Kadir, Experimental study of improved rheology and lubricity of drilling fluids enhanced with nanoparticles, *Applied Nanoscience*, 2018.
- [18] O. Anwar Bég, M. S. Khan, I. Karim, M. M. Alam and M. Ferdows, Explicit numerical study of unsteady hydromagnetic mixed convective nanofluid flow from an exponentially stretching sheet in porous media, *Applied Nanoscience*, vol 4 (8) ppl. 943-957, 2014

- [19] J. Buongiorno, Convective transport in nanofluids, *ASME J. Heat Transfer*, vol 128, pp. 240-250, 2006.
- [20] R. K. Tiwari, M. K. Das, Heat transfer augmentation in a two-sided lid-driven differentially heated square cavity utilizing nanofluids. *Int J Heat Mass Transfer*, vol 50, pp. 2002–2018, 2007.
- [21] M. J. Uddin, O. Anwar Bég and A. I. Ismail, Radiative-convective nanofluid flow past a stretching/shrinking sheet with slip effects, *AIAA J. Thermophysics Heat Transfer*, vol 29, 3, pp. 513-523, 2015.
- [22] O. Anwar Bég, M. Faisal M. d. Basir, M. J. Uddin, and A. I. Md. Ismail, Numerical study of slip effects on asymmetric bioconvective nanofluid flow in a porous microchannel with an expanding/contracting upper wall using Buongiorno's model, *J. Mechanics in Medicine and Biology*, vol 17 (5) 1750059 (28 pages), 2017.
- [23] N. A. Latiff, M. J. Uddin, O. Anwar Bég and A. I. M. Ismail, Unsteady forced bioconvection slip flow of a micropolar nanofluid from a stretching/ shrinking sheet, *Proc. IMechE- Part N: J. Nanoengineering and Nanosystems*, vol 230 (4) pp. 177–187, 2016.
- [24] A. B. Huda, N. S. Akbar, O. Anwar Bég, and M. Y. Khan, Dynamics of variable-viscosity nanofluid flow with heat transfer in a flexible vertical tube with propagating waves, *Results in Physics*, vol 7, pp. 413–425, 2017.
- [25] P. Rana, R. Bhargava, O. Anwar Bég and A. Kadir, Finite element analysis of viscoelastic nanofluid flow with energy dissipation and internal heat source/sink effects, *Int. J. Applied Computational Mathematics*, vol 3 (2), pp. 1421–1447, 2017.
- [26] D. Tripathi, A. Sharma and O. Anwar Bég, Joule heating and buoyancy effects in electro-osmotic peristaltic transport of nanofluids through a microchannel with complex wave propagation, *Advanced Powder Technology (Japan)* vol 29 (3), pp. 639-653, 2018.
- [27] F. T. Zohra, M. J. Uddin, A. I. Ismail, O. Anwar Bég and A. Kadir, Boundary layer anisotropic slip magneto-bioconvection flow from a rotating cone to a nanofluid with Stefan blowing effects, *Chinese J. Physics* vol 56 (1), pp. 432-448, 2018.
- [28] A. H. Elsheikhab, S. W. S. Mohamed, E. Mostafad, F.A. E. Mohamed and K. A. Alif, Applications of nanofluids in solar energy: A review of recent advances, *Renewable and Sustainable Energy Reviews*, vol 82(3), pp. 3483-3502, 2018.
- [29] M. J. Muhammad, I. A. Muhammad, N. A. C. Sidik, M. N. A.W.M. Yazid, R. Mamatb and G. Najafi, The use of nanofluids for enhancing the thermal performance of stationary solar collectors: A review, *Renewable and Sustainable Energy Reviews*, vol 63, pp. 226-236, 2016.
- [30] Z. Abdin, M. A. Alim, R. Saidur, M. R. Islam, W. Rashmi, S. Mekhilef and A. Wadib, Solar energy harvesting with the application of nanotechnology, *Renewable and Sustainable Energy Review*, vol 26, pp. 837-852, 2013.
- [31] G. Tegart, Priority areas for Australia's future, *Technological Forecasting and Social Change*, vol 76(9), pp. 1240-1246, 2009.
- [32] H. Wang, W. Yang, L. Cheng, C. Guan and Hua Yana, High performance nanofluids for solar energy, *Solar Energy Materials and Solar Cells*, vol 176, pp. 374-380, 2018.
- [33] F. Kiliç, T. Menlik and Adnan Sözen, Effect of titanium dioxide/water nanofluid use on thermal performance of the flat plate solar collector, *Solar Energy*, vol 164, pp. 101-108, 2018.
- [34] M. A. Sharafeldin and Gyula Grófa, Experimental investigation of flat plate solar collector using CeO₂-water nanofluid, *Energy Conversion and Management*, vol 155, pp. 32-41, 2018.
- [35] A. MeteGenc, M. A. Ezan and Alpaslan Turgut, Thermal performance of a nanofluid-based flat plate solar collector: A transient numerical study, *Applied Thermal Engineering*, vol 130, pp. 395-407, 2018.
- [36] T. Yousefi, F. Veysi, E. Shojaeizadeh, S. Zinadini, An experimental investigation on the effect of

- $\text{Al}_2\text{O}_3\text{H}_2\text{O}$ nanofluid on the efficiency of flat-plate solar collectors, *Renew. Energy*. vol 39, pp. 293-298, 2012.
- [37] M. H. Fard, M. Nasr Esfahany and M. R. Talaie, Numerical study of convective heat transfer of nanofluids in a circular tube two-phase model versus single-phase model, *Int. Commun. Heat Mass Transf.* vol 37, pp. 91-97, 2010.
- [38] G. Colangelo, E. Favale, P. Miglietta, M. Milanese, A. de Risi, Thermal conductivity, viscosity and stability of Al_2O_3 -diathermic oil nanofluids for solar energy systems, *Energy*, vol 95, pp. 124-136, 2016.
- [39] S. Salavati Meibodi, A. Kianifar, H. Niazmand, O. Mahian, S. Wongwises, Experimental investigation on the thermal efficiency and performance characteristics of a flat plate solar collector using SiO_2/EG -water nanofluids, *Int. Comm. Heat and Mass Transfer*. vol 65, pp. 71-75, 2015.
- [40] O. Mahian, A. Kianifar, A. Z. Sahin, S. Wongwises, Heat transfer, pressure drop, and entropy generation in a solar collector using $\text{SiO}_2/\text{water}$ nanofluids: effects of nanoparticle size and pH, *ASME J. Heat Transfer* vol 137 (6), 061011, 2015.
- [41] V. Bianco, O. Manca, S. Nardini, Performance analysis of turbulent convection heat transfer of Al_2O_3 water-nanofluid in circular tubes at constant wall temperature, *Energy*, vol 77, pp. 403-413, 2014.
- [42] M. A. Al-Nimr and Al-Dafaie, A. M. A., Using nanofluids in enhancing the performance of a novel two-layer solar pond, *Energy*, vol 68, pp. 318-326, 2014.
- [43] O. Mahian, A. Kianifar, A. Z. Sahin and S. Wongwises, Performance analysis of a mini-channel-based solar collector using different nanofluids, *Energy Conversion and Management*, vol 88, pp. 129-138, 2014.
- [44] S. Kuharat and O. Anwar Bég, ANSYS Fluent simulation of natural convection and radiation in a solar enclosure, *ICHTFM 2018: 20th International Conference on Heat Transfer and Fluid Mechanics*, Conference, The President Hotel, Istanbul, Turkey, August 16-17, 2018.
- [45] H. A. Daud, Q. Li, O. Anwar Bég and S.A. Ghani, Numerical study of flat plate film cooling effectiveness with different material properties and hole arrangements, *12th UK National Heat Transfer Conference 30th August -1st September*, School of Process Engineering, University of Leeds, UK, 2011.
- [46] O. Anwar Bég, B. Islam, M. D. Shamshuddin and T. A. Bég, Computational fluid dynamics analysis of moisture ingress in aircraft structural composite materials, *Int. J. Fluid Mechanics Research*, 2018. In press.
- [47] H. A. Daud, Q. Li, O. Anwar Bég and S.A. Ghani, CFD modeling of blowing ratio effects on 3-D skewed gas turbine film cooling, *11th Int. Conf. Advanced Computational Methods and Experimental Measurements in Heat Transfer*, Tallinn, Estonia, 14-16 July, 2010.
- [48] O. Anwar Bég, Armghan Zubair, Sireetorn Kuharat and Meisam Babaie, CFD simulation of turbulent convective heat transfer in rectangular mini-channels for rocket cooling applications, *ICHTFM 2018: 20th International Conference on Heat Transfer and Fluid Mechanics*, The President Hotel, Istanbul, Turkey, August 16-17, 2018.
- [49] ANSYS FLUENT Theory Manual, version 18.1, Swanson Analysis Systems, Pennsylvania, USA, 2018.
- [50] O. Anwar Bég, S. Kuharat and M. Shamshuddin, Computational fluid dynamics study of multi-mode heat transfer in spacecraft solar collectors with different radiative flux models, *Computational Thermal Sciences* (2018). In press.
- [51] M. Modest, *Radiation Heat Transfer*, MacGraw-Hill, New York, USA, 1993.
- [52] Puneet Rana, R. Bhargava and O. Anwar Bég, Finite element modelling of conjugate mixed

convection flow of Al_2O_3 -water nanofluid from an inclined slender hollow cylinder, *Physica Scripta*, vol 88, pp. 1-15, 2013.

- [53] A. J. Moghadam, M. Farzane-Gord, M. Sajadi and M. Hoseyn Zadeh, Effects of CuO/water nanofluid on the efficiency of a flat-plate solar collector, *Experimental Thermal and Fluid Science*, vol 58, pp. 9–14, 2014.
- [54] H. Maddah, M. Rezazadeh, M. Maghsoudi, and S. Nasiri Kokhdan, The effect of silver and aluminium oxide nanoparticles on thermophysical properties of nanofluids, *J. Nanostructure in Chemistry*, 3, article 28, 6 pages, 2013.

Biographical information

Miss Sireetorn Kuharat

was born in Thailand in 1993. She emigrated to Leigh, Lancashire UK in 2010. She graduated with a First-class honours degree in Aeronautical Engineering in 2016 at the University of Salford, specializing in rocket channel cooling simulation in her final year. In 2017 she obtained the MSc in Aerospace Engineering with distinction also at the University of Salford specializing in computational fluid dynamics of spacecraft solar collectors. She commenced her PhD study under the guidance of Dr. Anwar Bég in January 2018 and is investigating multiple configurations for nanofluid-based solar thermal absorption collectors. She is employing a variety of approaches in her research including ANSYS FLUENT codes, finite difference numerical methods and experimental testing. Her research has been featured at conferences and in several journals.



Dr. O. Anwar Bég was born in Dewsbury, Yorkshire, England in September 1969. He obtained a First-Class BEng (Hons) degree in Engineering (1992)

(winning the Jack Allen Prize for excellence in Fluid Mechanics) and a PhD in Computational Magnetohydrodynamics (1996), both from the University of Manchester. He then worked in industrial



consultancy for five years where he was involved with aero-structural analysis/dynamics and computational fire dynamics modelling. He attended the First MIT Conference in Computational Fluid and Solid Mechanics in 2001. He was Course Director of the BSc (Hons) in Fire Safety Engineering Sciences at Leeds Metropolitan University for five years, where he also taught engineering mathematics, fire dynamics, explosion sciences, thermo-fluids and acoustics. He then taught aerodynamics at BAE Systems, Riyadh, Arabia and was engaged in researching hypersonic and electromagnetic propulsion. He was subsequently Director of the MEng (Hons) degree in Aerospace Engineering at Sheffield Hallam University from 2007-2012 and won the SHU Distinguished Teaching Award in 2012 for contributions in propulsion, aerodynamics, rocket engineering and thermal sciences. After a further period in industry working in rocket propulsion simulation and biomimetic aerodynamics and marine hydrodynamics (2013-2016), he came to the University of Salford in March 2016 where he established new courses in computational fluid dynamics and aero-fluid mechanics and where he has led the research in multi-physical fluid dynamics, aero-thermophysics, nanofluid mechanics and biological propulsion. He has supervised over 20 MSc dissertations since 2016 in vortex rocket systems, autonautics (flying cars), aero-acoustics, magnetic swirl

propulsion, nano-drilling fluids for petroleum recovery, functional graded thermoelasticity, rocket nozzle design, peristaltic micro-pumps, nano-structural mechanics, corrosion protection and electrokinetic transport phenomena. He has also supervised numerous undergraduate projects in biomimetic aerodynamics, oil spill hazard simulation, fire dynamics, renewable energy systems, hybrid propulsion and landing gear dynamics. He has been an Associate Editor of the Journal of Mechanics in Medicine and Biology since 2010. In 2017 he was appointed as the UK Editor for the US-based Journal of Nanofluids. In Summer 2018 he won a Vice Chancellor Research Excellence Award for his substantial and sustained contributions to engineering sciences research. He has published 410 papers in many leading

internal journals, 30 conference articles (most recently at ICHTM: 2018, Istanbul, Turkey), six book chapters and five books in magnetohydrodynamics, micropolar fluid dynamics and the history of engineering science. He recently co-edited the book “Modelling and Simulation in Engineering Sciences”, published by Intech Press. His heroes in science are the late Professor A.C. Eringen, Turkish-American pioneer in engineering sciences (formerly of Princeton University, USA and founder of the Society of Engineering Science, 1962), Theodore Von Karman (founder of Caltech’s Jet Propulsion Laboratory and the “father of aerospace engineering”) and Professor Gary Flandro, one of the world’s leading combustion and rocket aero-acoustics pioneers (of the University of Tennessee Space Institute, USA).